

# Thermodynamic behavior of $^{57}\text{Fe}$ implanted into $\text{ZrO}_2(\text{Y})$ by CEMS and slow positron beam\*

Zhang Gui-Lin (张桂林), Yu Fang-Hua (俞方华)

(Shanghai Institute of Nuclear Research, the Chinese Academy of Sciences, Shanghai 201800)

Weng Hui-Min (翁惠民)

(University of Sciences and Technology of China, Hefei 230026)

and Zhang Xing-Hua (张行华)

(College of Material Science, Shanghai University, Shanghai 201800)

**Abstract** Using conversion electron Mössbauer spectroscopy (CEMS) and slow positron beam, the chemical state of  $^{57}\text{Fe}$  ( $100\text{ keV}$ ,  $3 \times 10^{16}\text{ cm}^{-2}$ ) implanted into  $\text{ZrO}_2$  containing 0.03 mole fraction  $\text{Y}_2\text{O}_3$  ( $\text{ZY}_3$ ) and its thermodynamic behavior during annealing process at  $200 \sim 500^\circ\text{C}$  are studied. For as-implanted sample, Fe chemical states of  $\text{Fe}^0$ ,  $\text{Fe}^{2+}$  and  $\text{Fe}^{3+}$  are observed, and assigned to the superparamagnetic metallic iron cluster, iron dimer (and trimer) and complex of the  $\text{Fe}^{3+}$  associated with cation vacancy (V) and oxygen, respectively. After annealing at  $400^\circ\text{C}$  the complexes of  $\text{Fe}^{3+}\text{-V}$  are mostly dissolved, and the prior phase to  $\alpha\text{-Fe}$  and  $\alpha\text{-Fe}$  nano-crystalline cluster are present in the sample. Meanwhile the mixed conducting of oxygen-ions and electrons in the  $\text{ZY}_3$  sample containing Fe appears, it may correlate with the different iron charge states and their relative amounts, in particular with the  $\alpha\text{-Fe}$  nano-granule.

**Keywords**  $^{57}\text{Fe}$  ion beam,  $\alpha\text{-Fe}$ , Nano-granule, Conversion electron Mössbauer spectroscopy, Positron annihilation Doppler broadening spectra

## 1 Introduction

The solid solution of  $\text{ZrO}_2$  with  $\text{Y}_2\text{O}_3$  is a good oxygen ion conducting electrolyte<sup>[1,2]</sup> at elevated temperature. Electron-ion mixing electrode could be formed on the surface layer in the  $\text{ZrO}_2(\text{Y})$  by Fe ion implantation, they help a very thin layer without sharp interface form between the top layer and the  $\text{ZY}_3$  specimen and save electrical power. The properties of the implanted material depend on the micro structure connecting with thermodynamic behavior of the implanted ions. Burggraaf *et al*<sup>[2]</sup> and Marest *et al*<sup>[3]</sup> studied thermodynamic process of the implanted iron in  $\text{ZrO}_2$  and  $\text{ZY}_3$  in vacuum and in argon atmosphere, respectively. But the RBS results were evidently different. Marest *et al*<sup>[3]</sup> found that Fe depth profile for the annealed sample at  $500^\circ\text{C}$  was obviously different from that for as-implanted. But Burggraaf *et al*<sup>[2]</sup> found that Fe depth profile did not change for the annealed sample, even after annealing at  $900^\circ\text{C}$ . However, they both found that fine clus-

ter  $\text{Fe}_2\text{O}_3$  was formed after annealing at  $400^\circ\text{C}$ . In order to keep the implanted Fe ions in low vacuum from oxidation during annealing process, we annealed samples in hydrogen atmosphere. Using CEMS and Doppler broadening spectra of slow positron annihilation radiation, we have studied the valence states and structural configurations for the as-implanted Fe ion, and their aggregation with annealing temperatures, obtaining the relationship between Fe nano-meter clusters and the electron conducting for the samples under study.

## 2 Experimental procedures

### 2.1 Samples

The samples of  $\text{ZY}_3$  were formed by mixing  $\text{Y}_2\text{O}_3$  (0.03 mole fraction) powder and  $\text{ZrO}_2$  powder homogeneously and pressing into a cake with a diameter of 20 mm, then sintering at  $1600^\circ\text{C}$  for 3 h and tempering at  $500^\circ\text{C}$  for 1 h.  $\text{ZY}_3$  samples were implanted with  $^{57}\text{Fe}^+$  beam (100 keV) at room temperature in  $1.33 \times 10^{-4}\text{ Pa}$  and its fluence is  $3 \times 10^{16}\text{ cm}^{-2}$ , corresponding

\*The Project Supported by National Climbing Plan A special subject

Manuscript received date: 1996-04-20

atom fraction is  $\sim 0.06$ , the implanted area is about  $1\text{ cm}^2$ . Finally, the isochronal thermal treatment was performed in hydrogen in sequence from 200 to  $500^\circ\text{C}$  for 30 min.

## 2.2 CEMS measurement

Mössbauer spectra were taken in back scattering geometry, measuring the conversion electron by resonant counter with 0.05 volume fraction  $\text{CH}_4$  in helium gas flow electron counter at room temperature. Mössbauer source is  $^{57}\text{Co}(\text{Pd})$  with 555 MBq. The isomer shift (IS) is relative to a metal iron.

## 2.3 Slow positron annihilation

The experiments were performed using a variable-energy positron beam of USTC<sup>[4]</sup>. The samples were mounted on the top of the bar with high voltages in the high vacuum ( $0.133\text{ mPa}$ ) target chamber. The FWHM of energy dispersion of slow positron was less than 2 eV, the energy could vary between 0~18 keV. The positron annihilation Doppler broadening spectra were measured by the intrinsic high pure Ge detector as a function of the positron energy( $E$ ) from 0.5 to 18keV. The data were analyzed in terms of the  $S$  parameter, which is the ratio of  $\gamma$ -ray counts at the central part of the 0.511MeV annihilation peak to the total counts contained in the whole peak.

# 3 Experimental results

## 3.1 CEMS of Fe in the as-implanted samples

Fig.1a presents CEMS spectra measured at room temperature of  $\text{ZY}_3$  sample implanted with  $^{57}\text{Fe}$  of 100 keV and with a dose of  $3\times 10^{16}\text{ cm}^{-2}$ . The Mössbauer parameters are shown in Table 1, which is obtained from fitting spectra with the least square procedure with the assumption of Lorentzian shape of Mössbauer lines. From the consistent fit, CEMS spectrum in Fig.1a can be decomposed to four quadrupole-split doublets and one singlet. The later can be ascribed to superparamagnetic metallic  $\alpha$ -Fe, due to its IS closes to zero. This viewpoint is consistent with those of Burggaaf<sup>[2]</sup> and Marest<sup>[3]</sup>. It can be found that the relative intensity (RI) of sextet for  $\alpha$ -Fe with ion energy of 15 keV and dose of  $8\times 10^{16}\text{ cm}^{-2}$  by Burggraaf *et al* is stronger than that obtained by Marest *et al* with ion energy of 100 keV and fluence of  $8\times 10^{16}\text{ cm}^{-2}$ . For our sample the concentra-

tion of Fe in  $\text{ZY}_3$  is smaller than those of their samples. Therefore, the probability of forming metallic iron ( $\alpha$ -Fe) grain with large size should be much smaller, i.e., the superparamagnetic peak maybe belongs to small iron clusters.

**Table 1** IS, QS,  $W$ (line width),  $H_f$  and RI as a function of annealing temperatures for the  $\text{ZrO}_2$  implanted with  $^{57}\text{Fe}$

		As-impl	200°C	400°C	500°C
I	IS/mm·s <sup>-1</sup>	-0.01	-0.02	-0.01	-0.01
	W/mm·s <sup>-1</sup>	0.38	0.45	0.50	0.46
	RI	0.06	0.07	0.06	0.02
II	IS/mm·s <sup>-1</sup>	0.20	0.21	0.19	0.19
	QS/mm·s <sup>-1</sup>	0.73	0.68	0.48	0.82
	W/mm·s <sup>-1</sup>	0.52	0.52	0.58	0.68
	RI	0.35	0.33	0.18	0.13
III	IS/mm·s <sup>-1</sup>	0.30	0.32	0.22	0.48
	QS/mm·s <sup>-1</sup>	0.93	0.73	0.95	0.96
	W/mm·s <sup>-1</sup>	0.75	0.74	0.42	0.51
	RI	0.34	0.37	0.13	0.11
IV	IS/mm·s <sup>-1</sup>	0.86	0.84	0.84	0.84
	QS/mm·s <sup>-1</sup>	0.77	0.77	0.77	0.77
	W/mm·s <sup>-1</sup>	0.67	0.66	0.66	0.66
	RI	0.06	0.07	0.11	0.04
V	IS/mm·s <sup>-1</sup>	1.12	1.07	1.07	1.04
	QS/mm·s <sup>-1</sup>	2.12	2.29	1.94	1.91
	W/mm·s <sup>-1</sup>	1.06	0.85	0.51	0.92
	RI	0.18	0.15	0.12	0.16
VI	IS/mm·s <sup>-1</sup>	-	-	0.24	0.25
	QS/mm·s <sup>-1</sup>	-	-	0.02	0.03
	$H_f/\text{kOe}$	-	-	199.3	208.4
	W/mm·s <sup>-1</sup>	-	-	0.83	0.48
	RI	-	-	0.40	0.23
VII	IS/mm·s <sup>-1</sup>	-	-	-	0.04
	QS/mm·s <sup>-1</sup>	-	-	-	0.001
	$H_f/\text{kOe}$	-	-	-	328.7
	W/mm·s <sup>-1</sup>	-	-	-	0.27
	RI	-	-	-	0.30

Four doublet components in the spectrum are divided to two groups. One is  $\text{IS}=0.2\sim 0.3\text{ mm/s}$  and  $\text{QS}=0.7\sim 0.9\text{ mm/s}$ . The other is  $\text{IS}=0.85\sim 1.12\text{ mm/s}$  and  $\text{QS}=0.70\sim 2.10\text{ mm/s}$ . These hyperfine parameters correspond to the typical high spin states of  $\text{Fe}^{3+}$  and  $\text{Fe}^{2+}$ , respectively. Comparing the experimental results with the binomial distribution of the implanted ions, it is found that some of iron ions implanted into  $\text{ZrO}_2$ <sup>[5]</sup>,  $\text{Al}_2\text{O}_3$ <sup>[6]</sup> and  $\text{MgO}_2$ <sup>[7]</sup> exist in the isolated ion state with  $\text{IS}=0.24\sim 0.4\text{ mm/s}$  and  $\text{QS}=0.4\sim 1.0\text{ mm/s}$ . These isolated  $\text{Fe}^{3+}$  ions are probably combined with the cation vacancies(V) and  $\text{O}^{2-}$  ions to form the complexes.

Shell - model calculations<sup>[8]</sup> of the stability

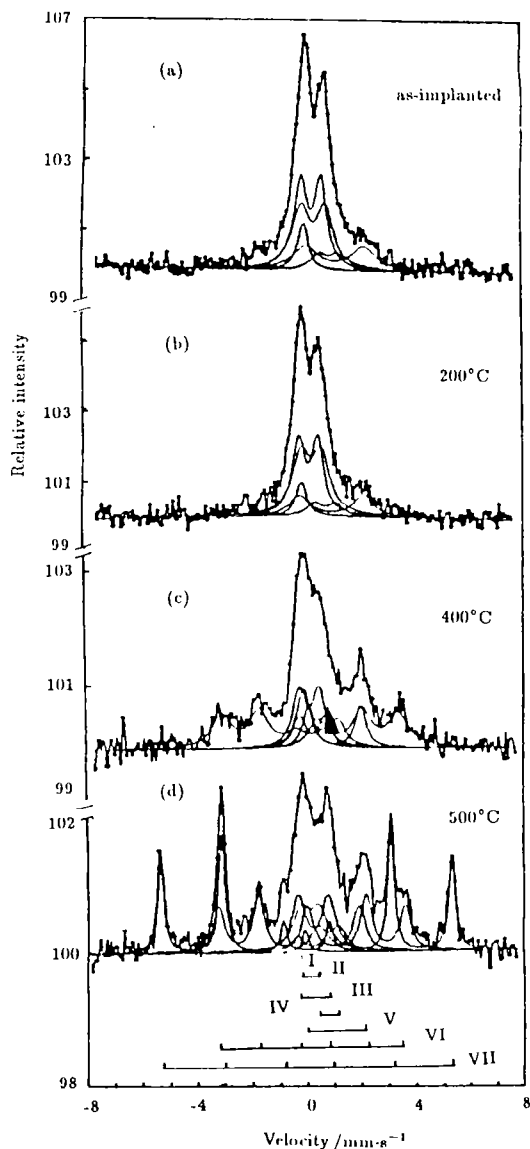


**Fig.1** CEMS for  $\text{ZrO}_2(\text{Y})$  implanted with  $^{57}\text{Fe}$   
 I- $\text{Fe}^0$ , II- $\text{Fe}_I^{3+}$ , III- $\text{Fe}_{II}^{3+}$ , IV- $\text{Fe}_I^{2+}$ , V- $\text{Fe}_{II}^{2+}$ , VI-Prior  
 phase to  $\alpha\text{-Fe}$  VII- $\alpha\text{-Fe}$

energy of various  $\text{Fe}^{3+}$ -vacancy complexes indicated that  $\text{Fe}^{3+}\text{-O}^{2-}\text{-V-O}^{2-}\text{-Fe}^{3+}$  trimer is the stablest configuration. It is also found that the local states of  $^{57}\text{Fe}$  in substrate were determined by electric neutral metal -vacancy configuration<sup>[5]</sup>, such as  $\text{Fe}^{3+}\text{-O}^{2-}\text{-V}$  or  $\text{V-O-Fe}^{2+}\text{-O-V}$  complexes. Therefore, it is not clear

yet for the  $\text{Fe}^{3+}$  configuration in the  $\text{ZY}_3$  samples. Maybe, several different configurations of  $\text{Fe-O-V}$  exist because two groups of Mössbauer parameters were found in this study. As it is well known that many oxygen vacancies ( $\text{V}_\text{O}$ ) in  $\text{ZrO}_2$  are formed by Y mixed in  $\text{ZrO}_2$ , e.g.  $\text{Y}_2\text{O}_3 \rightarrow 2\text{Y}_{\text{Zr}}^{3+} + \text{V}_\text{O} + 3\text{O}^{2-}$ . Therefore they must influence the configurations of  $\text{Fe}^{3+}$  ions. We assume that  $\text{Fe}_{II}^{3+}$  with larger IS is combined with more vacancies and less  $\text{O}^{2-}$  ions, compared to  $\text{Fe}_I^{3+}$  with smaller IS. We also can not exclude the possibility that  $\text{Fe}_{II}^{3+}$  may be  $\text{Fe}^{4+}$  ion which located in distorted  $\text{FeO}_6$  octahedral site, as isomer shift of  $\text{Fe}^{3+}$  is a little smaller than that of the typical isolated  $\text{Fe}^{3+}$  ions.

It is found that Fe ions implanted into  $\text{ZrO}_2$ <sup>[5]</sup>,  $\text{Al}_2\text{O}_3$ <sup>[6]</sup> and  $\text{MgO}$ <sup>[7]</sup> can formed two different  $\text{Fe}^{2+}$  ion sites,  $\text{Fe}_I^{2+}$  and  $\text{Fe}_{II}^{2+}$ , where  $\text{Fe}_I^{2+}$  represents iron in dimer,  $\text{Fe}_{II}^{2+}$  in trimer and other more complicated configurations. The IS and QS values for these components are close to the values in Table 1. So we presume that the doublet with IS = 1.12 and QS = 2.1 mm/s is attributed to  $\text{Fe}_{II}^{2+}$  and the doublet with IS = 0.86 and QS = 0.77 to  $\text{Fe}_I^{2+}$ .

### 3.2 Thermodynamic behavior of Fe implanted into $\text{ZY}_3$

After annealing at 200°C, RI for each component is nearly the same as that for as-implanted state (see Fig.2). Upon annealing at 400°C RI for  $\text{Fe}^{3+}$  decreased from 0.70 of the as-implanted to 0.30, in which RI of  $\text{Fe}_I^{3+}$  and  $\text{Fe}_{II}^{3+}$  decreased from 0.41 to 0.18 and from 0.29 to 0.125, respectively. Meanwhile a ferromagnetic phase prior to  $\alpha\text{-Fe}$  phase appeared<sup>[9]</sup>, it has a small hyperfine field,  $H_f = 199.3 \text{ kOe}$ . These results show that  $\text{Fe}^{3+}\text{-O-V}$  complexes began to decompose, a part of  $\text{Fe}^{3+}$  ions was reduced to  $\text{Fe}^0$ , then these atoms were gathered into small clusters by the interaction among  $\text{Fe}^0$  atoms.

After annealing at 400°C, about 0.40 of  $\text{Fe}^{3+}$  ions are reduced to  $\text{Fe}^0$ , but the relative amount of the  $\text{Fe}^{2+}$  component was nearly unchanged, it is probably as a result of competition between forming  $\text{Fe}^{2+}$  dimer or trimer from decomposed  $\text{Fe}^{3+}$  and transforming them to  $\alpha\text{-Fe}$ . Annealed up to 500°C, a ferromagnetic phase with sextet appeared in the Mössbauer spectrum,  $H_f = 329 \text{ kOe}$  and IS = 0.04 mm/s close to those of metallic Fe. Therefore, this magnetic

component should be assigned to  $\alpha\text{-Fe}$ . Meanwhile, the intensities of the superparamagnetic component and the magnetic component with small hyperfine field were reduced significantly. This result indicates that  $\alpha\text{-Fe}$  phase was trans-

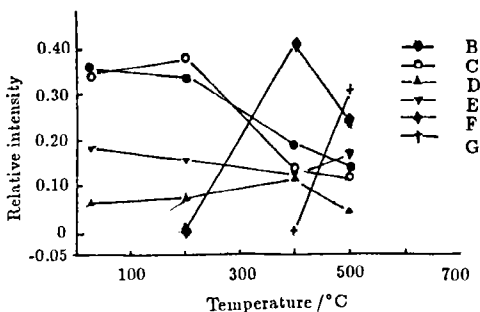


Fig.2 RI of various components as a function of annealing temperatures

B- $\text{Fe}_I^{3+}$ , C- $\text{Fe}_{II}^{3+}$ , D- $\text{Fe}_I^{2+}$ , E- $\text{Fe}_{II}^{2+}$ , F-Prior phase to  $\alpha\text{-Fe}$ , G- $\alpha\text{-Fe}$

### 3.3 Slow positron beam studies

Curve 1 in Fig.3 shows that  $S$  parameter for positron energy of 2~5 keV (corresponding to 20~90 nm in depth) is smaller than that for positron energy of 6~12 keV (corresponding to 120~360 nm in depth). It means that there exist more positron trapped centers in the inner layer than those on surface during sintering process of  $\text{ZrO}_3(\text{Y})$  samples. It can be attributed to Y element enriching, bringing about more un-intrinsic cationic vacancy<sup>[10,11]</sup> (trapped center) in the deeper region. For the curve 3 in Fig.3 there is a sharp increase in  $S$  parameter in 0.5~6 keV (2.2 ~ 120 nm). It indicated that  $^{57}\text{Fe}$  implantation produced a large amount of cationic vacancies, then the  $\text{Fe}^{3+}\text{-O}^{2-}\text{-V}$  complexes were formed. This result strongly supports the CEMS result mentioned in section 3.1. According to calculation by Trim program, the deepest depth for implanted  $^{57}\text{Fe}$  with 100 keV is about 40 nm underneath the surface, this value consists with the depth where the largest  $S$ -parameter was obtained from slow positron beam. Therefore the larger  $S$ -parameter indicates the more vacancy density produced by ion collision. The curve of  $\Delta S_{3-1}(=S_3-S_1)$  presents the difference between the iron implanted  $\text{ZY}_3$  and  $\text{ZY}_3$

formed from them. In addition,  $\text{Fe}^{3+}$  ions may be a complexes associated with vacancy and oxygen ion  $\text{O}^{2-}$  only with different configurations, because the annealing behaviors for both  $\text{Fe}_I^{3+}$  and  $\text{Fe}_{II}^{3+}$  are similar to each other.

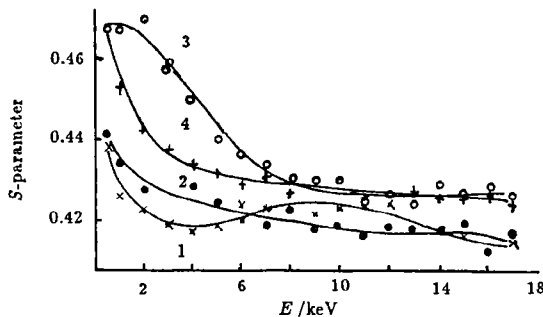


Fig.3 Doppler parameters  $S - E$  curves measured by slow positron beam

1.  $\text{ZY}_3$  unannealed
2.  $\text{ZY}_3$  annealed at  $500^\circ\text{C}$
3. As-implanted  $^{57}\text{Fe}$  in  $\text{ZY}_3$
4. Annealed at  $500^\circ\text{C}$  for  $^{57}\text{Fe}$  implanted  $\text{ZY}_3$

substrate. From the curve the positron trapped center profile produced by iron implantation is able to be obtained. The trapping centres in the outer layer approach to the results calculated by Trim program, but  $\Delta S$  in the inner (120 ~ 632 nm) is smaller due to lower concentration of Fe ions. It is also evident from the curve that vacancy density produced by ion collision is much higher than the un-intrinsic cation vacancy produced by Y doping. After annealing at  $500^\circ\text{C}$ , the difference between the  $S - E$  curve 2 for substrate  $\text{ZY}_3$  and the  $S - E$  curve 4 for  $^{57}\text{Fe}$  ion implanted  $\text{ZY}_3$  are rather small. It means that after annealing oxygen desorption on the surface of  $\text{ZY}_3$  and/or homogenizing of the micro structure of  $\text{ZY}_3$  took place for the substrate  $\text{ZY}_3$ , and the ion irradiation defects were recovered for the implantation sample and the trapping centers decreased. The difference between curves 2 and 4 is nearly constant,  $\Delta S_{4-2}=0.0012$ . The difference shows that there still exists a certain amount of  $\text{Fe}^{3+}\text{-O-V}$  complexes in the specimen after annealing at  $500^\circ\text{C}$ . This result is consistent with that of CEMS. The remained complexes probably need higher temperature for dissociation.

## 4 Discussion

For iron implanted  $\text{ZrO}_2$ ,  $\text{Al}_2\text{O}_3$  and  $\text{MgO}$

samples, it was found that under different annealing conditions the results could be quite different<sup>[5,6,7]</sup>, especially for annealing in vacuum and in air. As well known, iron atom is an element to be easily oxidized, even at depth of  $\sim 50\text{nm}$  by implantation with energy of  $100\text{keV}$ . Some of oxygen atoms can diffuse into the crystalline through crystal boundary or vacancies, oxidizing  $\text{Fe}^{2+}$  to  $\text{Fe}^{3+}$  that is so called internal oxidation.<sup>[12,13]</sup> For our sample  $\text{ZY}_3$ , all  $\text{Fe}^{2+}$  ions were oxidized into  $\text{Fe}^{3+}$  at  $550^\circ\text{C}$  in the mixture atmosphere of  $2.66\text{kPa}$  hydrogen and  $1.33\text{kPa}$  air. Therefore, high vacuum or hydrogen protection measures must be adopted in studying thermodynamic behavior of Fe ions implanted into sample.

Solid solution  $\text{ZY}_x$  is an excellent oxygen ion conducting electrolyte with high strength when the doped Y produces oxygen vacancy, and oxygen ions migrate between the vacancies. After doping Fe element into  $\text{ZY}_3$ , the  $\text{ZY}_3$  could become mixed conducting electrolyte.<sup>[14,15]</sup> The electron conducting is caused by electron transition between the electron charge states of Fe ions. For Fe doped  $\text{ZY}_3$  sample the electrical conductivity experiment<sup>[16]</sup> shows that the electrical conductivity at  $300^\circ\text{C}$  is  $3 \times 10^{-6} \Omega^{-1}\text{cm}^{-1}$ , it is one order of magnitude higher than that for the Fe undoped samples. Therefore we suppose that the larger conductivity might connect with  $\alpha\text{-Fe}$  cluster of small size formed during annealing. After forming a certain amount of Fe, electron conducting is induced by the transfer of charges among  $\text{Fe}^0$ ,  $\text{Fe}^{3+}$  and  $\text{Fe}^{2+}$ .

## 5 Conclusion

From the results of CEMS, Fe ions implanted into  $\text{ZY}_3$  sample exist in  $\text{Fe}^{3+}$ ,  $\text{Fe}^{2+}$  and  $\text{Fe}^0$  states.  $\text{Fe}^0$  resides in the form of cluster with superparamagnetic behavior. The  $\text{Fe}^{2+}$  ions are formed iron dimer and trimer. The  $\text{Fe}^{3+}$  ion is ascribed to the isolated Fe ion located in the environment without iron near neighbourhood, but associated with cationic vacancy and oxygen and formed  $\text{Fe}^{3+}\text{-V}$  or  $\text{Fe}^{3+}\text{-O}^{2-}\text{-V}$  complexes in  $\text{ZY}_3$ . Upon annealing at  $400^\circ\text{C}$  and  $500^\circ\text{C}$ , Fe valence states changed, meanwhile the  $\text{Fe}^{3+}\text{-O}^{2-}\text{-V}$  complexes were decomposed, vacancies disappeared mostly, and

Fe configuration changed. Under the annealing condition with dilute hydrogen  $\alpha\text{-Fe}$  with large size ( $> 5\text{nm}$ ) was formed due to preventing from Fe oxidation.  $S-E$  curves fully prove that a large amount of cationic vacancies were induced by Fe ion implantation, and their distribution corresponding to the implantation zone. After annealing at  $500^\circ\text{C}$ ,  $S-E$  curve shows that those vacancies disappeared mostly. So it provides a new evidence for assigning sites of Fe in  $\text{ZY}_3$ . At  $300^\circ\text{C}$  mixed conducting appeared in  $\text{ZY}_3$  sample. It probably correlates with different iron charge states, especially with amount of  $\text{Fe}^0$  compared with those of  $\text{Fe}^{2+}$  and  $\text{Fe}^{3+}$ .

## References

- 1 Weller M, Schubert H. J Am Ceram Soc, 1986; 69:573
- 2 Burggraaf A J, Scholten D, van Hassel B A. Nucl Instru Meth, 1988; B32:32
- 3 Marest G, Donnet C, Sawicki J A. Hyper Inter, 1990; 56:1605
- 4 Weng Hui-Min, Guo Xue-Zhe, Han Rong-Dia *et al.* Nucl Instr and Meth, 1991; A307:577
- 5 Sawicki J A, Marest G, Cox B *et al.* Nucl Instru and Meth, 1988; B32:79
- 6 Mchargue C J, Farlow G C, Sklad P S *et al.* Nucl Instr and Meth, 1987; B19/20:813
- 7 Perez A, Marest G, Sawickw B D *et al.* Phys Rev, 1983; B28:1227
- 8 Gourdin W II, Kingery W D, J Mater Sci, 1979; 14:2074
- 9 Zhang G L, Liu L F, Hu W.X *et al.* Phys Lett, 1986; A119:251
- 10 Forster M, Mundy J N, Schaefer H E. In: Positron annihilation, 8th ICPA, Singapore: World Scientific, 1989; 833
- 11 Shaefer H E, Forster M. Mater Sci Eng. 1989; A109:161
- 12 Groves G E, Fine M E. J Appl Phys, 1964; 35:3587
- 13 Zhang G L, Andreassen H, Boerma D D *et al.* Phys Rev, 1989; B39:1068
- 14 Miyayama Masuru, Yanagida Hiroaki, Asala Akiyoshi. Am Ceram Soc Bull, 1985; 64:660
- 15 Liou S S, Worell W L. Appl Phys, 1989; A49:25
- 16 Zheng Y M. An analysis of the phase structure in  $\text{ZrO}_2$  by Mössbauer spectroscopy and electric conductivity measurement for  $\text{Fe-Y-ZrO}_2$ . Master thesis, Shanghai University of Science and Technology, 1993